

Assessing ice margin fluctuations on differing timescales: Chronological constraints from Sermeq Kujatdleq and Nordenskiöld Gletscher, central West Greenland

Samuel E Kelley,^{1,2}  Jason P Briner² and Sandy L O'Hara²

The Holocene
2018, Vol. 28(7) 1160–1172
© The Author(s) 2018
Reprints and permissions:
sagepub.co.uk/journalsPermissions.nav
DOI: 10.1177/0959683618761541
journals.sagepub.com/home/hol


Abstract

The observational record of ice margin position reveals asynchrony in both the timing and magnitude of Greenland Ice Sheet (GrIS) margin fluctuations and illustrates the complex reactions of ice sheets to climatic perturbations. In this study, we reconstruct the timing and pattern of middle- and late-Holocene GrIS margin fluctuations at two locations, ~190 km apart, in central West Greenland using radiocarbon-dated sediment cores from proglacial-threshold lakes. Our results demonstrate that deglaciation occurs at both sites during the early Holocene, with the ice sheet remaining in a smaller-than-present ice margin configuration until ~500 years ago when it readvanced into lake catchments at both sites. At our northern site, Sermeq Kujatdleq, the late-Holocene advance of the GrIS approached maximum position during the past 280 years, with the culmination of the advance occurring at AD 1992–1994, and modern retreat was underway by AD 1998–2001. In contrast, field and observational evidence suggest that the GrIS at our southern site, Nordenskiöld Gletscher, has been advancing or stable throughout the 20th century. These results, in conjunction with previous work in the region, highlight the asynchronous nature of late-Holocene advances and subsequent modern retreat, implying that local variability, such as ice velocity or ice dynamics, is responsible for modulating ice margin response to changes in climate on these decadal to centennial timescales. Additional high-resolution records of past ice sheet fluctuations are needed to inform and more accurately constrain our predictions of future cryosphere response to changes in climate.

Keywords

Greenland Ice Sheet, ice dynamics, ice sheet reconstruction, lake core, late-Holocene, 'Little Ice Age', middle-Holocene, threshold lake

Received 7 June 2017; revised manuscript accepted 30 January 2018

Introduction

Global sea-level rise is a critical environmental and socio-economic issue facing today's society, with studies indicating that ice sheets will be the dominant driver of future sea-level rise (Stocker et al., 2013). It is estimated that the Greenland Ice Sheet (GrIS) will contribute decimeters to global sea-level rise by the end of the century (Meier et al., 2007; Pfeffer et al., 2008; Stocker et al., 2013). While forecasts of sea-level rise have been refined in recent years, estimates are still varied, spanning at least an order of magnitude (Price et al., 2011; Yoshimori and Abe-Ouchi, 2012). One factor contributing to the uncertainty in estimates of future sea-level rise is the dynamic behavior of ice sheet outlet glaciers in response to forecasted warming trends (Pfeffer et al., 2008). This dynamic behavior is exemplified in the variable magnitude of retreat exhibited by neighboring sectors of the GrIS margin during recent centuries, with retreat of kilometers documented at marine outlet glaciers next to stable land-terminating sectors of the ice margin (Kelley et al., 2015; Weidick, 1968, 1994). Given observations of present warming trends, especially in the high northern latitudes (Kaufman et al., 2009), analyzing the past behavior of ice sheets during the warming climate in the Arctic provides context for modern and historical observations of ice margin behavior. Specifically, glacial records from the early (11.7–8.2 ka) and middle (8.2–4.5 ka) Holocene,

derived from geologic observations of ice sheet growth and decay, can provide useful analogues for present and future ice sheet reactions to changes in climate.

Here, we present outlet glacier reconstructions built from lake sediment cores and sediment exposures that constrain middle- and late-Holocene ice margin fluctuations at two locations: one marine-terminating and one land-terminating in the Disko Bugt region of central West Greenland. We use our results, in conjunction with observational records (Weidick, 1968, 1994), to evaluate whether variable retreat observed along GrIS margins during the last century (Kelley et al., 2015; Levy et al., 2017; Weidick,

¹Department of Earth and Environmental Sciences, University of Waterloo, ON, Canada

²Department of Geology, University at Buffalo, NY, USA

Corresponding author:

Samuel E Kelley, Department of Earth and Environmental Sciences, University of Waterloo, 200 University Avenue West, Waterloo, ON N2L 3G1, Canada.

Email: samuel.kelley@uwaterloo.ca

1968, 1994) is a feature of the relatively short, decadal-scale, observational record, or whether this pattern is also evident over the longer, multi-centennial to millennial, timescales spanning the middle- and late-Holocene. We then postulate possible forcing mechanisms responsible for the observed asynchronous behavior of the modern GrIS margin.

Background

The deglaciation of the Disko Bugt region following the last glacial maximum is well understood, with studies constraining the early Holocene retreat across Disko Bugt to the mainland between ~11 and 10 ka (Kelley et al., 2013; Young et al., 2013). Cosmogenic exposure ages place the GrIS margin near present extent by 9.2 ka in northern Disko Bugt (Kelley et al., 2015), 7.4 ka near Jakobshavn Isbræ (Young et al., 2013), and 7.0 ka in southern Disko Bugt (Kelley et al., 2012). Geologic evidence from the time when the GrIS was smaller than the present, in contrast, is sparse. Studies dating marine macrofossils incorporated into till in the Jakobshavn area yield radiocarbon ages ranging from 6100 to 2300 cal. yr BP, suggesting reduced ice extent occurred during the middle- to late-Holocene (Weidick and Bennike, 2007; Young and Briner, 2015), with measurements of amino acid racemization of shell fragments in till giving a similar estimate, indicating the smallest extent of the GrIS occurring between 5 and 3 ka Briner et al. (2014). Sediment records from proglacial lakes place the minimum extent between 7000 and 1000 cal. yr BP, with local variability driven by catchment size and location (Briner et al., 2010; Kelley et al., 2012; Young and Briner, 2015).

The timing of the late-Holocene expansion of the GrIS in the Disko Bugt region is constrained by lake cores from isolation basins. These records indicate landscape submergence after ~3 ka, reflecting the late-Holocene ice sheet thickening and advance (Kelly, 1980; Long et al., 2011; Rasch, 2000; Weidick, 1993, 1996). However, an alternative interpretation of isolation basin records of relative sea level is that the 'j-shaped' curve reflects changes in the position of the GrIS forebulge (Long et al., 2009; Rasch, 2000; Rasch and Jensen, 1997), potentially indicating any isostatic loading associated with the most recent advance of the GrIS was minor.

Observational records reveal that GrIS outlet glaciers from Jakobshavn Isbræ north to Sermeq Avangnardleq achieved their late-Holocene maximum positions within the past 200 years, and have since undergone net retreat, while outlet glaciers south of Jakobshavn Isbræ, such as Alangordliup Sermia, Sarqardlip Sermia, and Nordenskiöld Gletscher, have exhibited little fluctuation of their ice margins over the same timeframe, with instances of net advance occurring since AD 1950 (Weidick, 1994). These historic records, combined with remote-sensing techniques (Csatho et al., 2008; Kelley et al., 2012), document the high degree of variability in recent fluctuations of the GrIS margin (Csatho et al., 2014), with significantly greater retreat noted at marine-terminating sectors of the ice sheet with respect to their land-terminating counterparts (Kelley et al., 2015; Kjær et al., 2012).

Study areas

The Disko Bugt region contains a diverse collection of ice-marginal environments forming a natural laboratory for examining ice-marginal fluctuations during the Holocene. Marine-terminating outlet glaciers, including Jakobshavn Isbræ which drains ~6.5% of the GrIS (Rignot and Kanagaratnam, 2006), are found in the northern and central part of the Disko Bugt region, with extended tracts of land-based GrIS margin more prevalent to the south. The two contrasting glacier systems selected for this study from the Disko Bugt region are: (1) Sermeq Kujatdleq, a marine-based glacier system in Torsukattak Fjord in northern Disko Bugt; and (2) Nordenskiöld Gletscher, a predominantly land-based outlet glacier located just south of Disko Bugt (Figure 1).

Sermeq Kujatdleq

Sermeq Kujatdleq is the southernmost of two outlet glaciers that feed into Torsukattak Fjord (Figure 1) and drains 20,667 km² of the GrIS with a peak surface velocity of 3056 m yr⁻¹ (Rignot and Mouginot, 2012). Torsukattak Fjord is an area of high relief, with fjord walls rising to >600 m a.s.l., and water depths exceeding 500 m in places (Rignot et al., 2010). Our examination of the middle- to late-Holocene fluctuations of Sermeq Kujatdleq are concentrated on the left-lateral flank of the glacier, where local deglaciation is constrained by a single ¹⁰Be exposure age at 10.0 ± 0.2 ka within the study area, and a pair of ¹⁰Be exposure ages at 9.3 ± 0.3 and 9.2 ± 0.2 ka located on the nearby nunatak separating Sermeq Kujatdleq from Sermeq Avangnardleq (Kelley et al., 2015). These ages are supported by a minimum-limiting radiocarbon age from a raised marine deposit of 8260 ± 60 cal. yr BP (Kelley et al., 2015). Our study utilizes sedimentological data from three lake basins: (1) Igdluuguaq, a proglacial lake located 2 km west of the ice margin; (2) Little Igy (informal name), a small lake dammed by an un-vegetated moraine near the ice margin; and (3) Arqataussap Tasia, an ice-marginal lake, which had partially drained at the time of our field investigations in August 2012 (Figure 2).

Nordenskiöld Gletscher

Nordenskiöld Gletscher, located ~35 km south of Disko Bugt (Figure 1), drains 13,602 km² of the GrIS and has a peak flow velocity of 173 m yr⁻¹ (Rignot and Mouginot, 2012). The landscape fronting Nordenskiöld Gletscher is characterized by rounded bedrock hills, and low-lying areas filled with till and glaciomarine sediments (Christoffersen, 1974). At present, Nordenskiöld Gletscher terminates in an estuary, with much of the glacier front resting on extensive sandflats emanating from the glacier terminus. A series of narrow channels connect the estuary at the glacier's front to Baffin Bay, located ~110 km to the west. A set of moraines is mapped 5–10 km outboard of the present ice margin (Weidick, 1968), and is correlative with the Fjord Stade moraines, a series of early Holocene moraines that marks a major readvance/standstill in central West Greenland (Weidick, 1968). The Fjord Stade moraines are attributed to the GrIS response to cold events at 9.3 and 8.2 ka (Lesnek and Briner, 2018; Young et al., 2013). In addition, a pair of un-vegetated moraines is located within ~100 m of the left-lateral margin of Nordenskiöld, though no moraines are present along the glacier terminus. A single ¹⁰Be exposure age from a boulder located between Pterodactyl lake (informal name) and the right-lateral margin of Nordenskiöld Gletscher indicates that local deglaciation occurred at 8.2 ± 0.2 ka (Figure 3; Kelley et al., 2015). This timing of local deglaciation is corroborated by a basal radiocarbon age from a non-glacial lake next to Pterodactyl lake, placing deglaciation before 7200 ± 400 cal. yr BP (Figure 3; Kelley et al., 2015). Our examinations of the middle- to late-Holocene fluctuations of Nordenskiöld Gletscher focus on the right-lateral margin of the glacier. Specifically, we focus on Pterodactyl lake, a large bedrock-controlled proglacial lake (approximately 3 km × 2.5 km), located 15 km northeast of the GrIS terminus at Nordenskiöld Gletscher. Pterodactyl lake receives glacial meltwater via a smaller ice-contact lake with a bedrock-controlled threshold, with an outlet on the western margin (Figure 3).

Methods

Lake sediment coring

Five lake sediment cores were collected from three lakes in the two study areas. Coring locations within each lake were selected using a Garmin GPSMAP 400 series GPS receiver connected to a dual-beam echo sounder. Coring was performed using a universal coring system (<http://www.aquaticresearch.com>) and a Nesje-style percussion-piston coring system (Nesje, 1992). Cores were driven into the lake sediment until the penetration rate slowed significantly, with no cores meeting hard refusal. Cores were drained

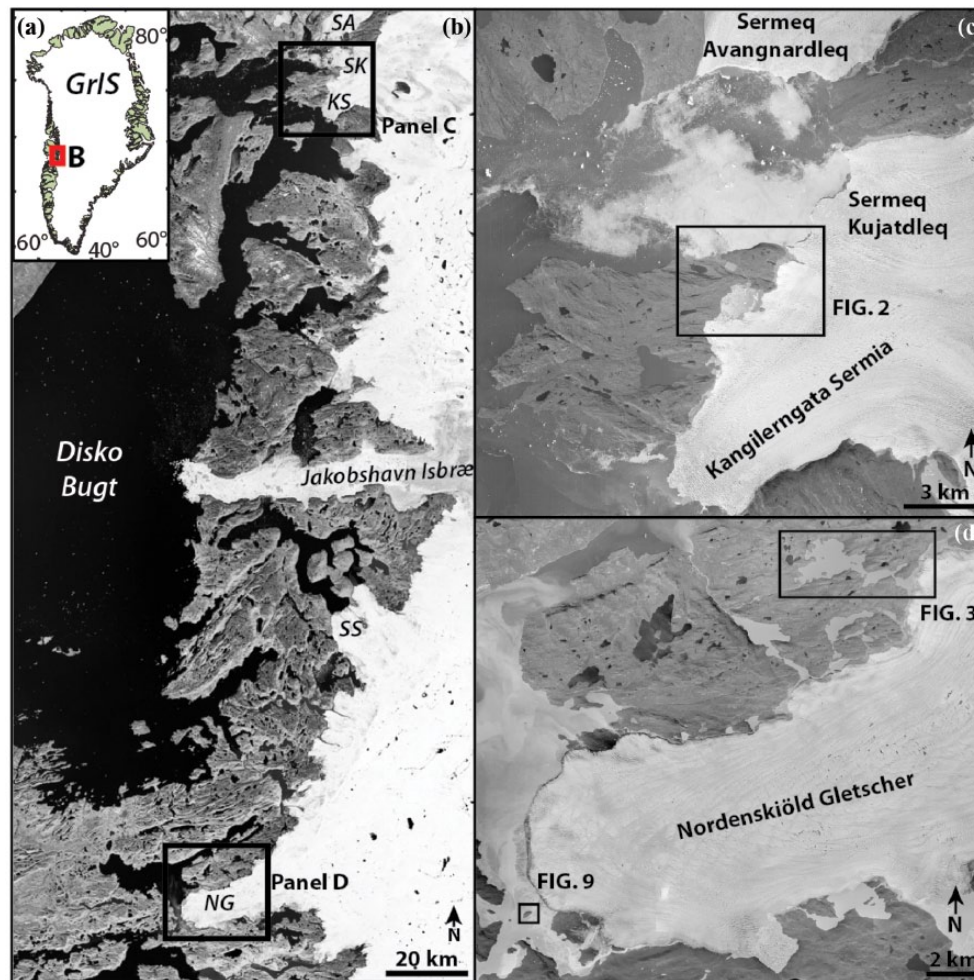


Figure 1. (a) Map showing the location of the Disko Bugt region within Greenland (box labeled B). (b) Composite Landsat image (Aug–Sept 1999) showing the Greenland Ice Sheet margin in the Disko Bugt region, with outlet glaciers mentioned in the text labeled (KS= Kangilerngata Sermia, NG=Nordenskiöld Gletscher, SA=Sermeq Avangnardleq, SK=Sermeq Kujalleq, SS=Sarqardlíp Sermia), as well as the location of the two study areas (boxes in (c) and (d)). (c, d) Close-up views of the two study areas, as well as the location of images in Figures 2, 3 and 9. The background image for (c) and (d) is a 1985 vertical aerial photograph.

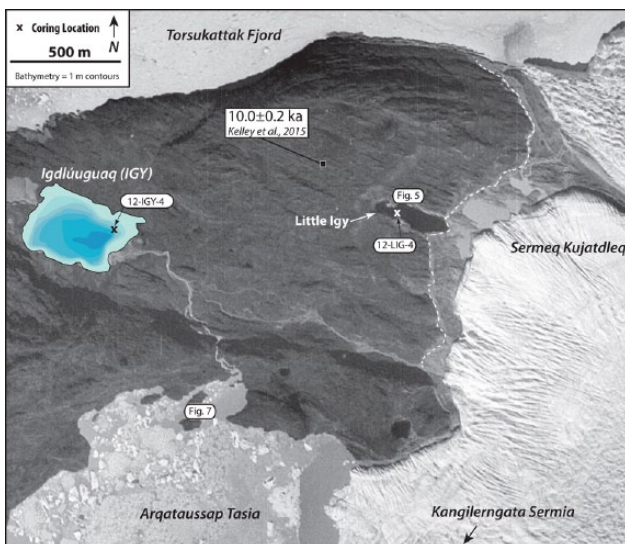


Figure 2. The Sermeq Kujatdleq study area, showing the location of the ^{10}Be sample from Kelley et al. (2015; black square) and corresponding age, the locations of Figures 5 and 7, and radiocarbon samples (rounded rectangles). Coring locations are marked by an 'x', with shading within Igdlúuuaq depicting the lake's bathymetry in 1 m contours to a maximum depth of 7 m. The short-dashed line on the right-hand side of the figure denotes the position of an unvegetated moraine referred to in the text. The background image is a 1985 vertical aerial photograph.

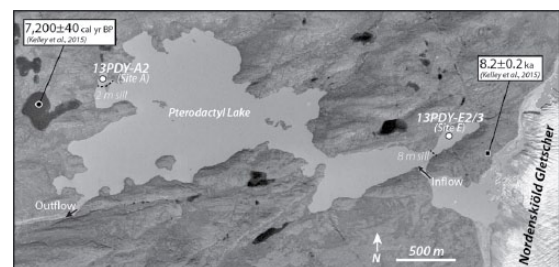


Figure 3. The Nordenskiöld Gletscher study area, showing the location of the inlet and outlet of Pterodactyl Lake, the location of the ^{10}Be sample (black square) and nearby basal radiocarbon sample (black circle) and corresponding ages from Kelley et al. (2015). The location of the two coring sites are noted with white circles (core logs are found in Figure 8). The sills separating the sub-basins from the rest of the lakes are marked by dashed lines, with sill depths given in italic text. The background image is a 1985 vertical aerial photograph.

vertically in the field with a small awl hole at the sediment–water interface, and zorbital (sodium polyacrylate powder) was used to dewater and stabilize the upper sediment surface. Cores were packed with floral foam and transported to the University at Buffalo where they were subsequently split, logged, and photographed. Measurement of magnetic susceptibility (MS) was performed on all cores at 5-mm intervals using a Bartington MS2E High-Resolution Surface Scanning Sensor connected to a Bartington Ms2 Magnetic Susceptibility Meter. Percent loss-on-ignition

Table 1. Sample information for radiocarbon ages.

Core/Site	Depth (cm)	Lab ID	Latitude (N)	Longitude (W)	Material dated	Fraction modern	$\delta^{13}\text{C}$ (‰PDB)
Torruskatak Fjord							
12-IGY-4	39	OS-99858	69.9743°	50.3525°	<i>Nostoc</i> sp.	0.9415 ± 0.0046	-18.20
12-IGY-4	141.5	OS-100052	69.9743°	50.3525°	Plant fragments	0.5782 ± 0.0027	-24.19
12-IGY-4	235	OS-99412	69.9743°	50.3525°	Shell fragment	0.4514 ± 0.0022	2.60
12-LIG-4	44.5	OS-100229	69.9760°	50.3067°	Plant fragments	0.9824 ± 0.0028	-25.40
Nordenskiöld Gletscher							
13-PDY-E2	36–36.5	OS-107097	68.4130°	50.8282°	Bulk Sediment	0.9024 ± 0.0041	-25.35
13-PDY-E3	28.5	OS-107096	68.4130°	50.8282°	<i>Drepanocladus</i> sensu lato sp.	0.5041 ± 0.0018	-33.01
13-PDY-E3	44.5–45	OS-107095	68.4130°	50.8282°	<i>Drepanocladus</i> sensu lato sp.	0.4623 ± 0.0019	-31.06
13-PDY-E3	88	OS-107092	68.4130°	50.8282°	Plant remains	0.4737 ± 0.0018	-30.88
13-PDY-E3	117.5	OS-107090	68.4130°	50.8282°	<i>Drepanocladus</i> sensu lato sp.	0.4628 ± 0.0018	-32.59
13-PDY-E3 ^a	190.5–191.5	OS-107088	68.4130°	50.8282°	<i>Daphnia</i> sp. and <i>Lepidurus arcticus</i> remains	0.4582 ± 0.0021	N/A
13-PDY-E3	132–133	OS-107091	68.4130°	50.8282°	<i>Rhabdocoela</i> <i>indet.</i> , <i>Lepidurus arcticus</i> , <i>Daphnia</i> sp., <i>Cladoc-</i> <i>era</i> <i>indet.</i> , <i>Chironomi-</i> <i>dae</i> <i>indet.</i>	0.6348 ± 0.0031	-23.32
13-PDY-A2	18–18.5	OS-107093	68.4191°	50.9163°	Plant remains	0.9871 ± 0.0036	-25.59
13-PDY-A2	27.5–28	OS-107099	68.4191°	50.9163°	<i>Sphagnum</i> sp., <i>Simocephalus vetulus</i> , <i>Rhabdocoela</i> <i>indet.</i> , <i>Alona</i> sp.	0.9312 ± 0.0036	-25.00
13-PDY-A2 ^a	126–126.5	OS-107094	68.4191°	50.9163°	<i>Drepanocladus</i> sensu lato sp.	0.4547 ± 0.0019	-26.77
Modern Dates							
Torruskatak Fjord							
12GRO-VEG-4	surface	OS-99779	69.9763°	50.3069°	Woody plant remains	1.1333 ± 0.0030	-27.04
12GRO-VEG-6	surface	OS-99780	69.9667°	50.3325°	Woody plant remains	1.3353 ± 0.0036	-27.52
12-LIG-3-12.5	12.5	OS-102468	69.9760°	50.3067°	Moss	1.0956 ± 0.0053	-30.61

Samples calibrated using Calib v.7.0, modern samples calibrated using CALIBomb software and are rounded to the nearest year AD. Marine macrofossils calibration corrected for a local reservoir effect of 140 ± 25 years from Lloyd et al. (2011). Modern ages calibrated using CALIBomb dataset.

^aDenote ages presented in Kelley et al. (2015).

(LOI) was measured on some cores at 5-mm resolution, by heating freeze-dried sub-samples to 550°C and determining the change in mass after heating, driven by the organic content of the sediment.

Macrofossils from both sediment cores and sediment exposures were washed in deionized water, freeze-dried, and submitted to the National Ocean Sciences Accelerator Mass Spectrometry Facility at Woods Hole Oceanographic Institute for radiocarbon dating. All ages were calibrated using the online program CALIB version 7.1 and the INTCAL13 or MarineCal13 datasets (Table 1; Stuiver et al., 2010). All of the radiocarbon ages presented in the text are in calendar years, rounded to the nearest decade, as the mean \pm half the two-sigma range. For ages that yielded multiple calibration solutions, the mean \pm half the two-sigma range of the highest probability solution is reported in the text, with all of the solutions available in Table 2, and the calibration plots presented in Supplementary Figure 1, available online.

Radiocarbon analyses that yielded modern results (those with high initial ^{14}C levels because of the onset of nuclear testing during the 1950s) were analyzed using the CALIBomb program (<http://calib.qub.ac.uk/CALIBomb/>; Reimer and Reimer, 2011). Results were calculated using the NH_zone1 dataset compilation and are reported as the one-sigma range (Table 1; Hua and Barbetti, 2007). This use of post-nuclear testing ^{14}C measurements

as a chronologic tool relies on the comparison of measured fraction modern within a sample to a dataset of measured atmospheric ^{14}C values. Additionally, as the ^{14}C is no longer uniformly distributed around the globe, region-specific calibration data (NH_zone1) are used to calibrate our ^{14}C measurements to years AD (Reimer et al., 2004). The region-specific calibration datasets comprise observed tropospheric ^{14}C levels, with supplemental data from tree rings and corals, which extend from 1950 to present, capturing the immediate pre- and post-bomb atmospheric ^{14}C levels in high resolution. For additional information on this topic, the reader is directed to Hua and Barbetti (2004) and Hua et al. (2013), with geosciences-specific applications discussed in Hua (2009).

Results and interpretations

Results: Igdluuguaq

Igdluuguaq (2 m a.s.l.) is a proglacial lake that currently receives meltwater from the left-lateral margin of Sermeq Kujatdleq via a ~2 km long meltwater stream (Figure 2). In addition, there is geomorphic evidence of a recently occupied outlet connecting Arqataussap Tasia to Igdluuguaq, which would be active during periods when Arqataussap Tasia is at a high-stand. Igdluuguaq is

Table 2. Calibration of radiocarbon ages.

Core/Site	Depth (cm)	Lab ID	Latitude (N)	Longitude (W)	Radiocarbon age (^{14}C yr BP)	Calibration solution(s) at 2σ (cal. yr BP) ^a	Highest probability solution (mean $\pm 2\sigma$)
Torruskatak Fjord							
12-IGY-4	45	OS-99858	69.9743°	50.3525°	485 \pm 50	336–348 (1), 456–563 (88) , 592–637 (11)	510 \pm 50
12-IGY-4	141.5	OS-100052	69.9743°	50.3525°	4400 \pm 40	4857–5062 (92) , 5113–5118 (<1), 5185–5215 (5), 5222–5238 (1), 5241–5267 (2)	4960 \pm 100
12-IGY-4	235	OS-99412	69.9743°	50.3525°	6390 \pm 40	6575–6834 (100)	6720 \pm 130
12-LIG-4	44.5	OS-100229	69.9760°	50.3067°	145 \pm 25	4–39 (18), 62–119 (21), 123–152 (12), 169–232 (32) , 242–281 (17)	200 \pm 30
Nordenskiöld Gletscher							
13-PDY-E2	36–36.5	OS-107097	68.4130°	50.8282°	825 \pm 35	680–792 (100)	740 \pm 60
13-PDY-E3	28.5	OS-107096	68.4130°	50.8282°	5500 \pm 30	6217–6238 (6), 6272–6324 (80) , 6328–6350 (4), 6367–6395 (9)	6300 \pm 30
13-PDY-E3	44.5–45	OS-107095	68.4130°	50.8282°	6200 \pm 35	6997–7180 (93) , 7193–7240 (7)	7090 \pm 90
13-PDY-E3	88	OS-107092	68.4130°	50.8282°	6000 \pm 30	6749–6768 (5), 6772–6914 (94) , 6917–6927 (1)	6840 \pm 70
13-PDY-E3	117.5	OS-107090	68.4130°	50.8282°	6190 \pm 30	6989–7176 (100)	7080 \pm 90
^a 13-PDY-E3	190.5–191.5	OS-107088	68.4130°	50.8282°	6270 \pm 35	7029–7043 (1), 7070–7077 (<1), 7087–7095 (1), 7097–7111 (1), 7155–7272 (97)	7210 \pm 60
13-PDY-E3	132–133	OS-107091	68.4130°	50.8282°	3650 \pm 40	3866–4088 (100)	3980 \pm 110
13-PDY-A2	18–18.5	OS-107093	68.4191°	50.9163°	105 \pm 20	24–49 (14), 52–141 (59) , 220–262 (28)	100 \pm 40
13-PDY-A2	27.5–28	OS-107099	68.4191°	50.9163°	575 \pm 30	530–568 (36), 584–648 (64)	620 \pm 30
^a 13-PDY-A2	126–126.5	OS-107094	68.4191°	50.9163°	6330 \pm 35	7168–7324 (100) , 7403–7407 (<1)	7250 \pm 80
Modern Dates						CALIBomb calibration (years AD)	
Torruskatak Fjord							
12GRO-VEG-4	Surface	OS-99779	69.9763°	50.3069°	Modern	1992–1994	
12GRO-VEG-6	Surface	OS-99780	69.9667°	50.3325°	Modern	1962 or 1976–1978	
12-LIG-3-12.5	12.5	OS-102468	69.9760°	50.3067°	Modern	1998–2001	

^aCalibrated solutions, with bold italicized text noting the highest probability solution; probabilities expressed as percentages given in parentheses for each range.

a single basin lake reaching a maximum depth of 6.2 m, with a bedrock-controlled outlet on the western margin of the lake at ~ 2 m a.s.l. The sediment core from Igdlúguaq (12-IGY-4; 69.9731° N, 50.3525° W) was collected in 5.2 m water depth on the northeastern side of the lake using a Nesje-style piston corer and is 235 cm long (Figure 4). The stratigraphy comprises three primary units: one, a basal minerogenic unit; two, a middle unit of gyttja; and three, an upper minerogenic unit. Unit 1 is 90 cm long, characterized by elevated MS values ranging from 142 cgs to near zero (mean of 21.9 cgs) and less than 4% organic matter (mean of 1.2%). The lowest 22 cm of the core comprises sand with silt lenses, which is overlain by 68 cm of massive gray silt. The contact between Unit 1 and Unit 2 is sharp and highlighted by a distinct dark brown layer of finely laminated gyttja with a sharp drop in MS values, and a transition from near zero percent organic matter below the contact to >20% organic matter immediately above the contact (Figure 4). Unit 2 is 104-cm thick and contains weakly laminated gyttja, with high percent organic matter ranging from 9% to 38% (mean of 23%), and MS value near zero. The contact between Units 2 and 3 appears sharp, characterized by a distinct rise in MS values and drop in percent organic material up the core to near zero. Unit 3, the uppermost unit, is 41-cm thick and is composed of massive silt with MS values ranging from 236 to 11 cgs, with the lowest values at the base of the unit, rising to 100 cgs 5 cm above the Unit 2/3 contact. Notably, near the top of Unit 3 is a thin organic band, located 8 cm below the top of the core, which is marked by a distinct drop in MS of 40 cgs (from 130 to 90 cgs).

Three samples were extracted from core 12-IGY-4 for radiocarbon dating to provide temporal control for sedimentologic changes seen in the core (Figure 4; Table 1). A shell fragment from the base of the core (235 cm depth) yields a calibrated age of 6710 \pm 130 cal. yr BP (6390 \pm 40 ^{14}C yr). A sample of organic-rich sediment from just above the Unit 2/Unit 1 contact (141.5 cm depth) yields an age 4960 \pm 100 cal. yr BP (4400 \pm 40 ^{14}C yr). Macrofossils of small algae colonies, *Nostoc* sp., collected from just above the Unit 3/2 contact at a depth of 39 cm yield an age of 510 \pm 50 cal. yr BP (485 \pm 50 ^{14}C yr).

Results: Little Igy basin

Little Igy is a proglacial lake located ~ 250 m west of the left-lateral margin of Sermeq Kujatdleq (Figure 2). Little Igy is dammed by a fresh-appearing, un-vegetated, moraine at its eastern end. The lake is 420 m \times 120 m, reaches a depth of ~ 3 –4 m (wind conditions prevented a comprehensive bathymetric survey), and drains to the east, toward the ice margin, through a gap in the moraine. A prominent lichen-free band encircled the lake to a height of ~ 2 m above the lake surface in August 2012 (Figure 5). Dead *Betula* sp. shrubs rooted in growth position above the 2012 lake level, yet below the 2-m trimline, yield a 'modern' age of AD 1992–1994. The collected shrubs were covered with a thin layer of silt and were common both above and slightly below the present lake level.

A 52-cm-long core, 12-LIG-4, was collected from a depth of 3.4 m in the western end of Little Igy using a universal coring device (Figures 2 and 4). The stratigraphy comprises two primary

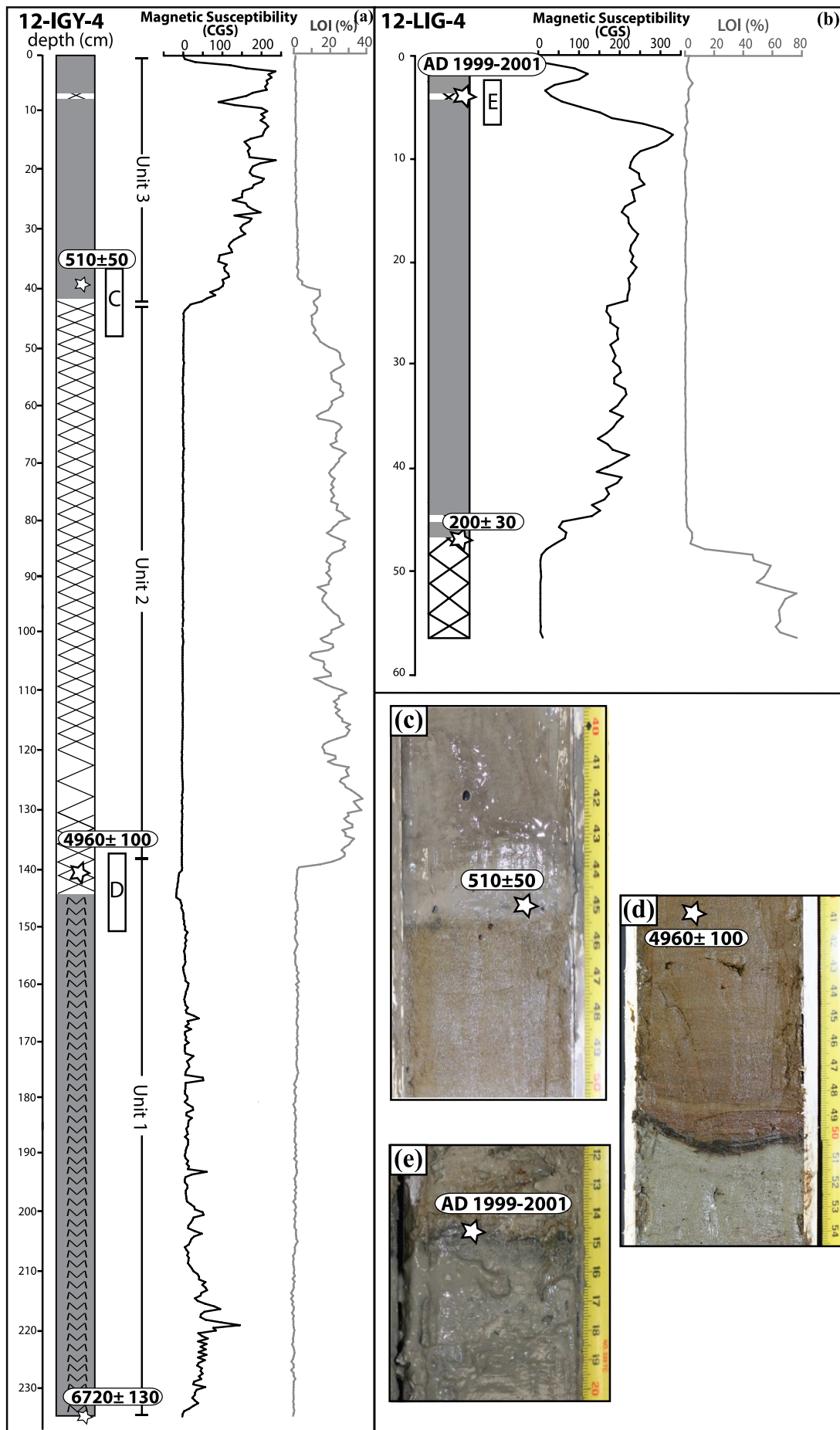


Figure 4. (a) (12-IGY-4) and (b) (12-LIG-4): Lake sediment core logs, radiocarbon ages (in cal yr BP), magnetic susceptibility (black line), and loss on ignition (gray line) measurements from the cores collected in Igy and Little Igy, respectively. The hachured pattern indicates organic-rich sediment; solid gray pattern reflects minerogenic sediments; “M” denotes inferred marine sediments; white boxes indicate the position of core photographs displayed in panels (c), (d), and (e). Note: Ruler on the left of each photo does not equal total depth.



Figure 5. View to the north across Little Igy lake, with person for scale (~180 cm), showing the lichen kill zone across the lake, and the dead shrubs (*Betula* sp.) in the foreground. Inset image shows a close-up of drowned, rooted shrubs (*Betula* sp.) that were sampled for radiocarbon dating.



Figure 7. Top photograph shows the northern basin of Arqataussap Tasia where sample 12GRO-VEG-6 was collected, view to the southeast. Note the paleo-shoreline in the photo behind the people (dotted line). Lower photograph shows the stratigraphic context for radiocarbon sample, with inferred lake sediments (light gray sediment) overlying a buried soil (tan sediment).

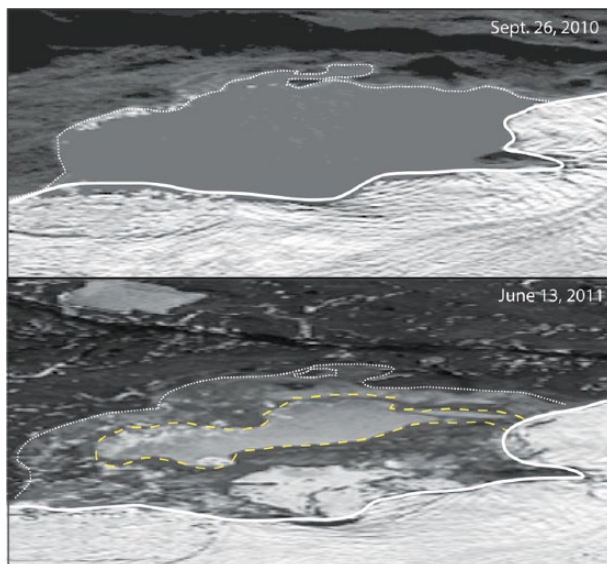


Figure 6. Cropped oblique satellite images from Digital Globe showing Arqataussap Tasia before and after the most recent draining event. The solid white line shows the ice margin position, the dotted white line shows the lake high-stand position, and the yellow dashed line shows the lake low-stand position.

units: one, a basal peat unit; and two, an upper minerogenic unit. Unit 1 is 8-cm thick and is characterized by abundant fibrous plant material (peat). LOI measurements on Unit 1 yield values that rise up core from 78% organic matter at the base of the unit to 14% organic matter at the top of the unit. Unit 2 is 44-cm thick and is composed of silt, with two prominent bands of fibrous plant

material at 43 and 4 cm depths (Figure 4). Above the uppermost organic band, the minerogenic sediment changes in color from gray to tan and exhibits lower MS values and slightly higher percent organic matter than the minerogenic sediment at 5–40 cm depth within Unit 2. Two macrofossil samples were collected from the core for radiocarbon dating. The lower sample, from the top of Unit 1 (44.5 cm), yields an un-calibrated age of 145 ± 50 ^{14}C yr (Tables 1 and 2). Calibration of this age yields five solutions ranging in probability from 12% to 32%, with possible solutions ranging from 0 to 280 cal. yr BP, with the highest probability solution of 200 ± 30 cal. yr BP. The upper sample collected for radiocarbon analysis, from the upper organic band in Unit 2 (4 cm), yields a modern age, with a post-bomb calibration of AD 1998–2001 (Tables 1 and 2).

Results: Arqataussap Tasia

Arqataussap Tasia is an ice-contact lake that is dammed by the GrIS margin between Kangilerngata Sermia and Sermeq Kujatdleq (Figure 2). When the lake is at a high-stand, it drains to the north over a bedrock-controlled outlet and into Igdlúguaq. During field investigations in August of 2012, the lake basin was partially drained of water. Digital Globe satellite imagery reveals that the most recent draining of the lake took place between 26 September 2010 and 6 June 2011 (Figure 6). At the time of our field investigations, a ~60-m vertical difference existed between the lake surface and a well-defined shoreline, as evidenced by a transition from a fully vegetated landscape above to one devoid of living vegetation below. In the northern portion of the lake basin, below the raised-shoreline, woody terrestrial plant fragments were found in growth position draped with gray silt, inferred to be glaciolacustrine

sediments (Figure 7). Stratigraphic sections that were dug revealed no deeper occurrence of lake sediment in the subsurface. A radiocarbon-dated sample of woody plant material found in growth position yielded a modern age of AD 1962 or AD 1976–1978 (Table 1).

Interpretations: Sermeq Kujatdleq area

^{10}Be ages constrain retreat of the GrIS to near the present margin's extent to 9.3 ± 0.1 ka on the nunatak on the right-lateral margin of Sermeq Kujatdleq and to 10.0 ± 0.2 ka on the left-lateral margin of Sermeq Kujatdleq (Kelley et al., 2015). Minimum-limiting constraints on continued deglaciation come from the sediment core retrieved from Igdlúguuaq, 12-IGY-4 (Figure 4). An age of 6710 ± 130 cal. yr BP from the base of the core indicates a minimum time of ice margin retreat from the lake basin. A transition from minerogenic sedimentation to organic sedimentation within the lake occurred before 4960 ± 100 cal. yr BP. We interpret this transition to be the basin's emergence from a turbid glaciomarine environment into a lacustrine environment because of isostatic rebound. This interpretation is supported by local deposits of marine sediments above the elevation of the lake, a shell fragment found at the base of the core, and the presence of a well-defined anoxic (dark colored) layer at a depth of 154 cm. This type of anoxic layer is defined by Long et al. (2011) to be a sedimentological isolation contact (Figure 4). This interpretation also fits with local relative sea-level records (Long et al., 1999), which indicate that relative sea level in the area dropped to near present levels at ~ 5 ka. While the change in sedimentation in this basin does not directly reflect a change in ice margin position as classically interpreted in threshold lakes (Briner et al., 2010; Daigle and Kaufman, 2009; Kaplan et al., 2002; Karlén, 1976), the presence of organic sedimentation indicates that Sermeq Kujatdleq had retreated out of the catchment of Igdlúguuaq sometime prior to ~ 5000 years ago. Therefore, the best local constraints on deglaciation in the area are derived from the basal age in core 12-IGY-4 of 6710 ± 130 cal. yr BP, as well as a radiocarbon date of 8260 ± 60 cal. yr BP and ^{10}Be exposure ages of 10.0 ± 0.2 within the study area and ages of 9.3 ± 0.3 and 9.2 ± 0.2 ka from a nearby nunatak (Kelley et al., 2015). In core 12-IGY-4, the upper change in sedimentation from organic to minerogenic reflects the late-Holocene advance of Sermeq Kujatdleq back into the Igdlúguuaq catchment after 510 ± 50 cal. yr BP.

Further evidence of the late-Holocene advance comes from Little Igy lake, where an advance of Sermeq Kujatdleq dammed the lake during the late-Holocene. We note that the Little Igy basin sits topographically above the modern terminus of Sermeq Kujatdleq; thus, in the current configuration, ice-marginal changes are likely driven both by marginal retreat as well as ice sheet thinning, processes that are shown to occur in tandem in West Greenland (Kjær et al., 2012). We interpret the transition from peat to minerogenic sediment, dated to 200 ± 30 cal. yr BP, as indicating the advance of the glacier that caused the former bog to fill with glaciogenic sediment. Though, we note that the calibration of this age yields solutions ranging from 0 to 280 years; thus, it does not provide tight control on the timing of the late-Holocene advance. That said, it does provide a constraint on an advance occurring during the past 300 years, allowing for a possible correlation to cooling associated with the 'Little Ice Age' ('LIA'; AD 1250–1900). A further constraint on the local position of the GrIS margin is derived from the Arqataussap Tasia basin. A radiocarbon age on the rooted shrub collected in the basin is inferred to provide a maximum constraint on the initial filling of the lake basin to its largest extent at AD 1962 or AD 1976–1978. At present, the ice margin position at Arqataussap Tasia is likely very similar to the ice margin position for the initial lake filling, given that the lake recently drained. We believe the radiocarbon age from the basin constrains the advance of the GrIS to near the present ice margin to the late 20th century. In addition, the presence of a lake high-stand in

Arqataussap Tasia from AD 1962 or 1976–1987 to 2011 provides a local constraint on the time when the GrIS was in a position to dam the lake to its high-stand and, thus, when the ice sheet was more extensive than at present.

Age control on the maximum late-Holocene ice sheet configuration comes from dead shrubs dated to AD 1992–1994 in the Little Igy basin. We identify two possible geomorphic interpretations for the event which killed the shrubs: (1) a rise in lake level is caused by encroachment of the GrIS margin that dammed the basin and deposited the un-vegetated moraine, and (2) a rise in lake level is caused by routing of additional ice-marginal runoff into Little Igy lake. If interpretation 1 is true, the age of AD 1992–1994 constrains the damming of Little Igy lake, thus constraining the maximum position of the GrIS. If interpretation 2 is correct, changes in lake level are related to local hydrology rather than the position of the GrIS margin.

An organic-rich horizon at 12.5-cm depth in the core from Little Igy lake yields a modern radiocarbon age of AD 1998–2001. Above the organic horizon, the sediment changes in color, and has higher LOI values and lower MS. We interpret this change in sediment character to be tied to the retreat of the GrIS off the moraine at the eastern end of Little Igy lake, with the meltwater source becoming more distal to our core site. Information from the Little Igy basin leads us to the interpretation that the GrIS margin advanced through the late 20th century. This interpretation of GrIS behavior is supported by historical evidence (Weidick, 1994), which places the GrIS margin at a maximum position at Sermeq Kujatdleq in AD 1992–1994, with net retreat following.

Results: Nordenskiöld Gletscher area

Pterodactyl lake is a multi-basin lake on the right-lateral margin of Nordenskiöld Gletscher (Figure 3). Pterodactyl lake currently receives glacial meltwater from Nordenskiöld Gletscher via a bedrock-controlled threshold on a smaller ice-marginal lake. Three cores were retrieved from two sub-basins in the northwest and northeast corners of Pterodactyl lake.

Two cores, 13-PDY-E2 and 13-PDY-E3, were recovered from a depth of 18.4 m in a sub-basin (site E) near the inflow to Pterodactyl lake. An 8-m-deep sill separates the sub-basin from the rest of Pterodactyl lake. 13-PDY-E2 was collected using a universal coring device and is 109 cm long (Figure 8). The stratigraphy comprises three primary units: one, a basal gyttja unit; two, a middle unit that grades from silt below to gyttja above; and three, an upper minerogenic unit. Unit 1 is characterized by laminated gyttja, is 44-cm thick, with ~ 0.5 -cm thick layers of silt at 93 and 84 cm depths. MS measurements within Unit 1 are consistently less than 5 cgs. Unit 2 is 32-cm thick and comprises a sequence that gradually changes from minerogenic sediment in the lower portion of the unit to gyttja at the top with falling MS values, from 24 cgs at 65 cm depth to 2 cgs at 33 cm depth, following the change in sediment. Unit 3 is a 32-cm thick unit of massive silt with MS values rising upward through the unit from 10 cgs at 32 cm to 120 cgs at 4 cm depth. A single bulk sample of organic sediment was extracted for radiocarbon dating from the top of the gradational sequence in Unit 2, at 31 cm depth. The sample yields an age of 740 ± 60 cal. yr BP (Tables 1 and 2; Figure 8).

The second core from the same sub-basin (site E), 13-PDY-E3, was collected using a Nesje-style piston coring device and is 244-cm long (Figure 8; Nesje, 1992). The stratigraphy comprises four primary units: one, a basal sand unit; two, a silt unit; three, a series of four sequences; and four, an upper unit of silt. Unit 1 is 29-cm thick and comprises massive sand with three 1-cm thick silt lenses at 234, 231, and 225 cm depth. Unit 2 is 21-cm thick, characterized by massive silt and fluctuating MS, which range from 60 to 180 cgs. Unit 3 is 191-cm thick, with four gradational sequences that have a lower component that is dominated by minerogenic

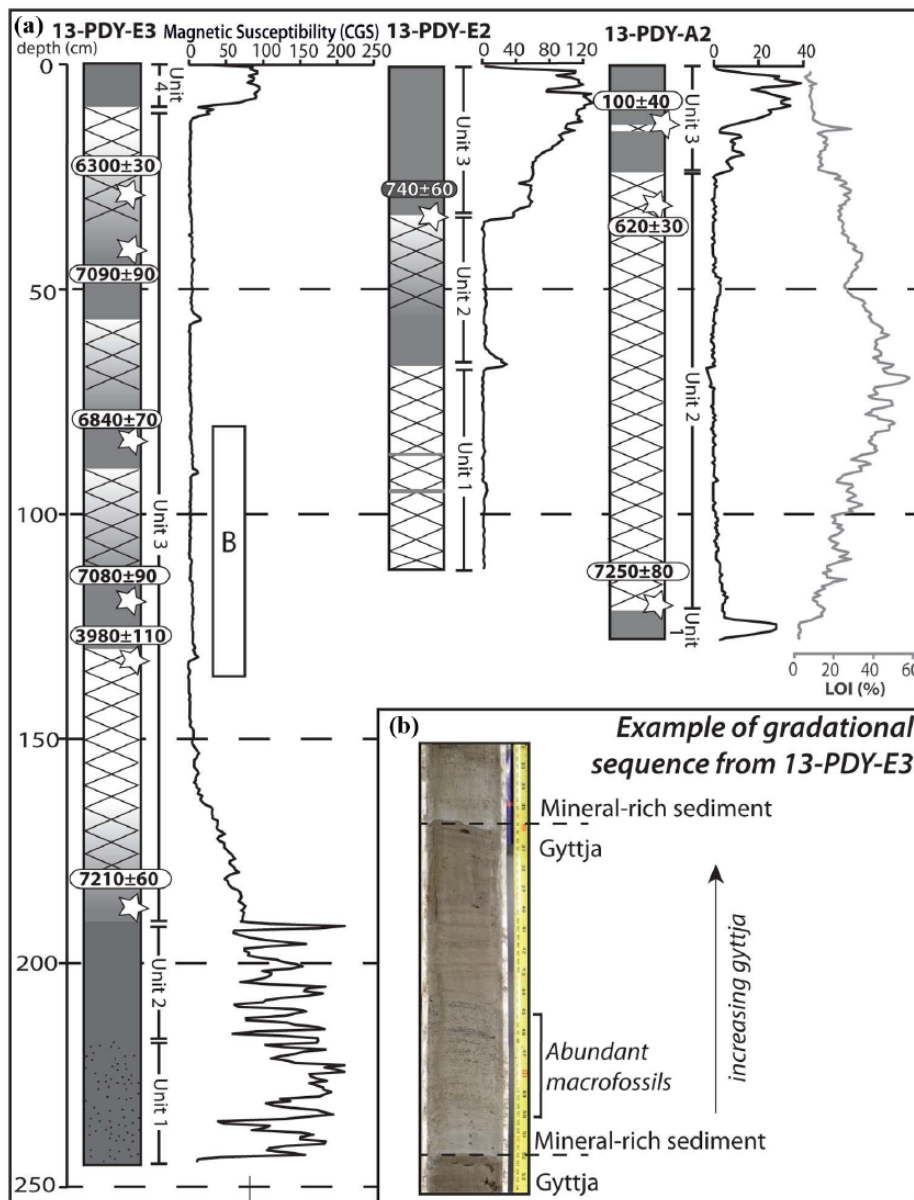


Figure 8. (a) Lake sediment cores from the Nordenskiöld Gletscher area, radiocarbon ages (in cal yr BP), magnetic susceptibility (black line; upper axis), and loss on ignition (gray line; lower axis). The hachured pattern indicates organic-rich sediment; solid gray shading reflects minerogenic sediments. Radiocarbon ages in white ovals are derived from macrofossils, while radiocarbon ages in gray ovals are derived from bulk sediment samples. The white rectangle indicates the position of the photo in (b). (b) Photograph demonstrating one of the gradation sequences observed in 13-PDY-E3, with annotations to denote sedimentological changes.

sediment with numerous macrofossils, which grades upward into an upper gyttja section with decreasing minerogenic material defined by falling MS values upward through the sequence. The gradational sequences are 65, 40, 45, and 47 cm in thickness, from the lowermost sequence to uppermost. Unit 4 is 10-cm thick characterized by massive silt. Six macrofossil samples were collected from core 13-PDY-E3 at depths 28.5, 44.5–45, 88, 117.5, 132–133, and 191 cm yielding ages of 6300 ± 30 cal. yr BP (5500 ± 30 ^{14}C yr), 7090 ± 90 cal. yr BP (6200 ± 35 ^{14}C yr), 6840 ± 70 cal. yr BP (6000 ± 30 ^{14}C yr), 7080 ± 90 cal. yr BP (6190 ± 30 ^{14}C yr), 3980 ± 110 cal. yr BP (3650 ± 40 ^{14}C yr), and 7210 ± 60 cal. yr BP (6270 ± 35 ^{14}C yr), respectively (Tables 1 and 2; Figure 8).

Core 13-PDY-A2 was collected using a universal coring device from a sub-basin in an ice-distal area of the lake at ~5 m depth (Figure 8). A 2-m-deep sill separates the sub-basin that was cored from the rest of the lake. The core is 126-cm long and has three primary units: one, a basal minerogenic unit; two, a middle gyttja unit; and three, an upper minerogenic unit. Unit 1 is 4-cm thick and comprises silt with MS values ranging from 15 to 29 cgs, and

<2% organic matter. Unit 2 is 99 cm of massive gyttja containing intervals of abundant macrofossils of plant material such as mosses, *Sphagnum*, and *Drepanocladus*, as well as organisms such as *Simocephalus vetulus*, *Rhabdocoela*, and *Alona*. MS values fall from 10 cgs at the base of the unit to 1 cgs at 102 cm depth and remain below 1 cgs for the rest of the unit. LOI measurements within Unit 2 yield organic content between 8% and 29%. Unit 3 comprised a massive silt that is 22 cm in thickness with a 0.5-cm-thick, macrofossil-rich horizon at 18 cm depth. This unit is defined by elevated MS values, an average of 17 cgs, with the exception of the macrofossil-rich horizon, which is marked by a sharp drop in MS to 3 cgs. LOI measurements within the macrofossil-rich horizon are also elevated at 14% organic matter, with organic content ranging from 8% to 2% within the rest of Unit 3. Macrofossils extracted for radiocarbon dating from Unit 2, just above the lower contact (126–126.5 cm depth) and below the upper contact (27.5–28 cm depth), yield ages of 7250 ± 80 cal. yr BP (6330 ± 35 ^{14}C yr) and 620 ± 30 cal. yr BP (575 ± 30 ^{14}C yr), respectively. A macrofossil sample from the upper macrofossil-rich horizon at 18–18.5



Figure 9. Photograph of the terminus of Nordenskiöld Gletscher taken in August 2013. Note the deposition of glacial sediments onto living tundra and the lack of moraine fronting the glacier.

cm depth in Unit 3 yields an un-calibrated age of 105 ± 20 ^{14}C yr, which generates three calibration solutions ranging in probability from 14% to 59% and in age from 20 to 260 years; the highest probability solution is 100 ± 40 cal. yr BP (Tables 1 and 2).

Interpretations: Nordenskiöld Gletscher

A single ^{10}Be age constrains the retreat of Nordenskiöld Gletscher to near the present ice margin configuration on its right-lateral margin at 8.2 ± 0.2 ka and is supported by a ^{10}Be age of 8.3 ± 0.2 ka located 5 km west of the terminus (Kelley et al., 2015). Basal radiocarbon ages from a nearby non-glacial lake provide additional minimum-limiting constraints on the timing of local deglaciation by 7200 ± 120 cal. yr BP (Kelley et al., 2015). Sediment cores from Pterodactyl lake indicate that the GrIS retreated out of the Pterodactyl lake watershed by 7230 ± 30 cal. yr BP ($n = 2$; mean \pm stand deviation of basal ages from 13-PDY-E3 and 13-PDY-A2). Cores 13-PDY-E3 present a complex stratigraphy. In a typical threshold lake, changes from minerogenic to organic sedimentation are interpreted to mark the ice margin retreating out of a lake's catchment, with the reverse stratigraphy indicating an advance of the ice margin into a lake's catchment. If this logic were followed for core 13-PDY-E3, the interpretation would be that the GrIS fluctuated across the catchment threshold of Pterodactyl lake four times since deglaciation. However, the six radiocarbon ages from this core suggest a more complex depositional environment (Figure 8). Given the relative homogeneity of the ages from core 13-PDY-E3, we interpret this core to represent a mass wasting event within the sub-basin. Four of the six ages are from macrofossils within the minerogenic portions of their respective gradational sequences, with all of these ages falling within 370 years of each other. The remaining two macrofossil-derived ages, located in gyttja-rich parts of the sequence, are younger than lower ages in the same respective sequences. We postulate that the gradational sequences of Unit 3 represent a subaqueous slump, where the slope failed within the minerogenic unit, with slump blocks comprising the same stratigraphy being stacked during transport and deposition. If this interpretation is correct, Unit 3 represents four sequences of the same stratigraphy ranging in age from ~ 7000 to ~ 4000 years.

Based on this interpretation, we suggest that the lowest date from core 13-PDY-E3 is undisturbed and relates to the GrIS margin retreat from the Pterodactyl lake catchment. This point is supported by similar basal radiocarbon dates from core 13-PDY-A2, and a basal radiocarbon age from a non-glacial lake located proximal to Pterodactyl lake (Figure 3; Kelley et al., 2015). We infer the same scenario for core 13-PDY-E2, with the core penetrating a different portion of the slump deposit. We treat the radiocarbon age from 13-PDY-E2 with caution, as it is from bulk sediment and consider it a maximum limiting age on the advance of the

Nordenskiöld Gletscher in the Pterodactyl lake catchment. It has been shown in studies from West Greenland that bulk sediment may give erroneously old ages in comparison to macrofossil-based ages by 100 ± 400 years (Bennike et al., 2010; Kaplan et al., 2002).

We infer that core 13-PDY-A2 was unaffected by slumping as it was collected from a sub-basin over 3 km away. As such, we use the classical interpretation of threshold lakes for this core (Briner et al., 2010; Daigle and Kaufman, 2009; Kaplan et al., 2002; Karlén, 1976). Middle-Holocene retreat of the GrIS margin is observed in the core, reflected as a sharp transition from silt below to gyttja above, and is constrained prior to 7250 ± 80 cal. yr BP. The late-Holocene advance of the GrIS into the Pterodactyl catchment is observed in core 13-PDY-A2 as a transition from organic gyttja below to minerogenic sediments above. The contact is constrained by a radiocarbon age of 620 ± 30 cal. yr BP. A thin organic-rich layer higher in the core suggests a brief cessation of glacial-meltwater contribution to the lake around 100 ± 40 cal yr BP, indicating a possible short-lived recession of the Nordenskiöld Gletscher. Another explanation for organic sedimentation at this time is that lake level dropped below the 2-m-deep sill at the mouth of the sub-basin because of a reduction in meltwater input from the GrIS. A lowering of lake level would isolate the sub-basin from the proglacial Pterodactyl lake, causing a cessation in minerogenic sediment deposition. The sediment record indicates that the right-lateral margin of Nordenskiöld Gletscher has remained in the Pterodactyl catchment since sometime after 620 ± 30 cal. yr BP. This is corroborated by fresh-appearing moraines along the lateral margins of Nordenskiöld that are located <100 m from the ice margin, suggesting only minor lateral retreat or thinning has occurred since a maximum late-Holocene extent.

Historical and remote-sensing records indicate that Nordenskiöld Gletscher has been stable or advancing since AD 1950 (Weidick, 1968, 1994). This evidence, in addition to the lack of a moraine or trimline marking the culmination of the late-Holocene advance fronting the ice margin, as occurs across much of the region, infers that the system is at or is still advancing to its late-Holocene maximum extent. We note the difference between the ice margin locations on the laterals versus the terminus relative to the late-Holocene maximum position and attribute this to deepening of the glacial trough as described by Kaplan et al. (2009). In fact, observations at the terminus of Nordenskiöld Gletscher in 2013 documented that the terminus is currently advancing onto living tundra (Figure 9). Additionally, shell fragments present in the dirty ice at the glacier's terminus indicate ongoing erosion at the base of the glacier via freeze-on of underlying marine sediments.

Discussion

Comparison of middle- to late-Holocene records

This study demonstrates the contrasting response of GrIS outlet glaciers to climate forcing over different time periods. At both sites, the middle-Holocene recession of the GrIS margin to a smaller-than-present ice margin configuration occurred between 8 and 7 ka. In turn, late-Holocene expansion of the GrIS was underway at both sites by 500 years ago, with the ice margin advancing into currently proglacial lake catchments. Notably, the most recent behavior, of the GrIS, is markedly different between the two sites, with retreat occurring at Sermeq Kujatdleq and expansion underway at Nordenskiöld (Figure 10; Weidick, 1994). We suggest that this juxtaposition, synchronous middle- and late-Holocene retreat and late-Holocene advance fluctuations and asynchronous modern behavior, indicates that the spatiotemporal relationships seen in our reconstructions may be a factor of the timeframe over which the ice margin behavior is viewed. We demonstrate a relative synchronicity in the fluctuation of the GrIS margin on millennial and centennial timescales, yet the asynchronous behavior is observed on decadal timescales, such as the modern disparity seen in our two study areas, with Sermeq Kujatdleq retreating and Nordenskiöld advancing. This pattern of

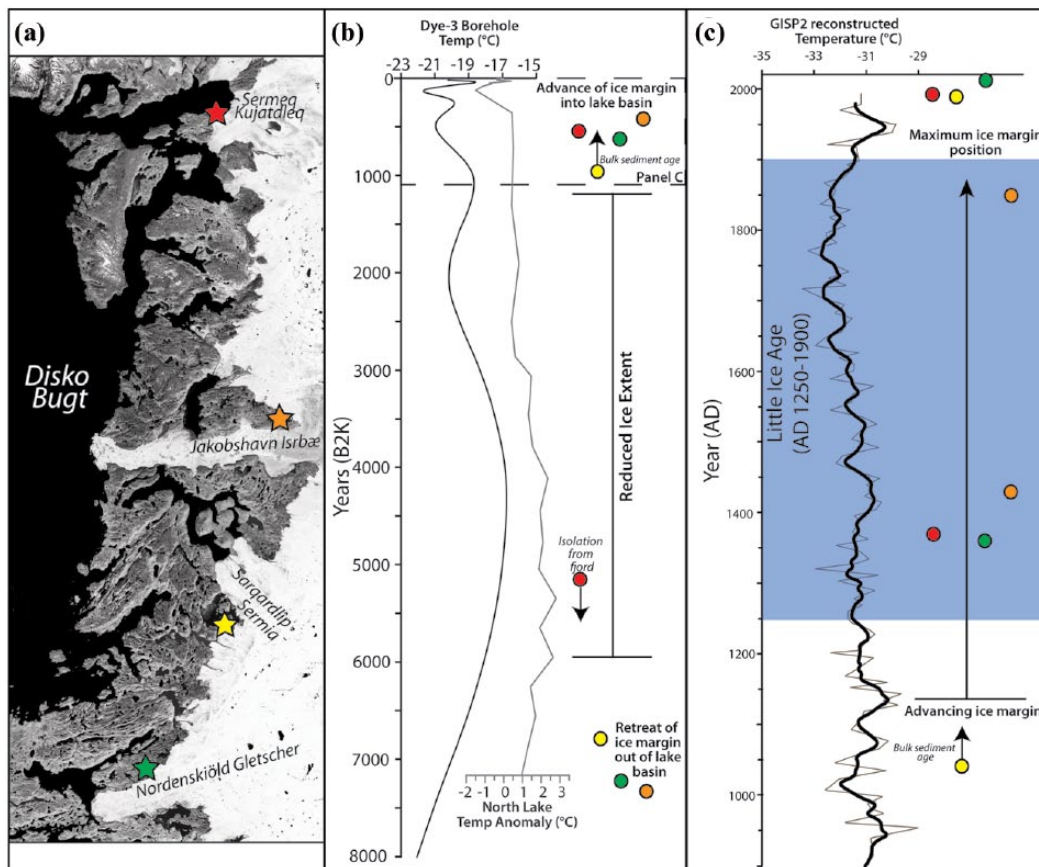


Figure 10. (a) The location of four threshold lakes in the Disko Bugt region. The northern- (red star) and southern-most sites (green star) are from this study, while the data from Jakobshavn Isbræ (orange star) is reported in Briner et al. (2010), and the site south of Sarqardlíp Sermia (red star) is detailed in Kelley et al. (2012). (b) Chronology of GrIS recession and advance from four Disko Bugt region threshold lakes, with circle color corresponding to the stars on the map. Ages are plotted versus Dye-3 borehole temperature (Dahl-Jensen et al., 1998) and reconstructed July air temperature anomalies from North Lake (also located at the orange star in (a)), inferred from chironomids as described in Axford et al. (2013). (c) Detailed view of threshold lake chronology of GrIS Neoglacial advance and retreat plotted versus a 30-year running average of reconstructed temperature from the GISP 2 ice core (Kobashi et al., 2011), with ages on timing of the maximum position from Weidick (1996). Blue shaded area depicts the timing of the Little Ice Age. This figure is available in color online at <http://journals.sagepub.com/home/hol>

contrasting modern ice margin behavior is well-documented across west Greenland (Kelley et al., 2012; Kjær et al., 2012; Weidick, 1994). As we assume climate forcing is relatively uniform across the region, factors inherent to the glacier systems must be responsible for driving the varying behavior on decadal timescales.

One of the local driving factors may be ice flow velocity. Previous work has postulated linkages between surface velocity and glacier response to climate forcing (Bamber et al., 2007), with the ‘perturbation theory’ stating that the local response time of a glacier is the inverse of the local velocity (Nye, 1960). Thus, higher velocity glaciers should have a closer temporal coupling with changes in climate forcing than slower glaciers. If the late-Holocene maximum position is the result of ‘LIA’ cooling, the correlation between ice margin setting and response time holds true to our study. We demonstrate that the faster flowing glacier, Sermeq Kujatdleq (3056 m yr^{-1}), achieved a maximum position in the late 20th century, and the slower glacier, Nordenskiöld Gletscher (173 m yr^{-1}), is still advancing toward its late-Holocene maximum position (Rignot and Mouginot, 2012). This demonstrates that both glacier system reactions are out of phase with peak ‘LIA’ cooling, with the slower flowing glacier system, Nordenskiöld, exhibiting the larger lag in reaction to climatic forcing.

Disko Bugt region Holocene ice margin fluctuations

We examine our results in the wider context of two additional outlet glaciers within the Disko Bugt region where the middle- and late-Holocene ice margin behavior is well-constrained (Figure 10; Briner

et al., 2010; Kelley et al., 2012; Weidick and Bennike, 2007). Jakobshavn Isbræ is currently the fastest flowing glacier in the world, achieving a peak flow velocity of $17,100 \text{ m yr}^{-1}$ (Joughin et al., 2014). The GrIS margin retreated behind the historical limit locally at $7.4 \pm 01 \text{ ka}$ (Young et al., 2013), and retreated out of the catchment of a threshold lake (transitioned from proglacial to non-glacial in the late 1960s; Briner et al., 2011) on the northern margin of Jakobshavn Isfjord by $7300 \pm 120 \text{ cal. yr BP}$ (Briner et al., 2010). The late-Holocene expansion of Jakobshavn Isbræ is recorded in a proglacial lake catchment north of the fjord with a change in sedimentation occurring by $390 \pm 80 \text{ cal. yr BP}$ (Briner et al., 2011), and historical evidence places the ice margin at its late-Holocene maximum by AD 1850 (Weidick, 1968). A net retreat of $\sim 40 \text{ km}$ has been observed between AD 1963 (Briner et al., 2011) and present (Weidick and Bennike, 2007).

Sarqardlíp Sermia is an outlet glacier located $\sim 50 \text{ km}$ south of Jakobshavn Isbræ and $\sim 70 \text{ km}$ north of Nordenskiöld Gletscher that has achieved a peak flow velocity of 251 m yr^{-1} (Figure 10; Rignot and Mouginot, 2012). Middle-Holocene retreat of Sarqardlíp Sermia behind its present position occurred at $7.0 \pm 0.1 \text{ ka}$ (Kelley et al., 2012). The late-Holocene constraints on the past extent of Sarqardlíp Sermia come from the Tininnilik basin, an ice-dammed lake that drains on a 7- to 10-year period (Kelley et al., 2012; Weidick and Bennike, 2007). The advance of Sarqardlíp Sermia reached an extent similar to today, damming the Tininnilik basin ~ 300 years ago. Maximum ice extent is documented between AD 1985 and 1997, based on observations at

Tinnilik, the Sarqardlíp Sermia terminus, and the neighboring basin of Qinngap Ilulialeraa (Kelley et al., 2012; Weidick, 1994).

The records from Sarqardlíp Sermia and Jakobshavn Isbræ illustrate similar behavior on millennial and centennial timescales to that of Sermeq Kujatdleq and Nordenskiöld Gletscher. All glaciers retreated behind the present ice margin position in the middle-Holocene; indeed, this pattern is seen throughout West Greenland (Cronauer et al., 2016; Kelley et al., 2015; Larsen et al., 2014; Levy et al., 2012). Late-Holocene advances occurred at all sites between 600 and 300 years ago, with the GrIS margin advance documented through changes in proglacial lake sedimentation (Briner et al., 2010; Kelley et al., 2012). On decadal timescales, the ice margin fluctuations are not synchronous in the sign or magnitude of ice margin change. Jakobshavn Isbræ has retreated tens of kilometers since AD 1850, while Sermeq Kujatdleq and Sarqardlíp Sermia retreated tens of meters since the late 20th century, and Nordenskiöld Gletscher has been advancing since at least AD 1950. These records demonstrate that four outlet glaciers in the Disko Bugt region exhibit asynchronous behavior on decadal timescales. This suggests that ice dynamics unique to each glacier catchment play a dominant role in driving ice margin fluctuations on shorter (decadal) timescales, thus implying that variability in the response of the GrIS to climate change because of local ice dynamics also is on the order of decades rather than centuries or millennia.

Furthermore, we see that faster flowing, marine-terminating, outlet glaciers have responded more quickly to warming following the end of the 'LIA', indicating a lag in the response of slower, land-based, sectors of the ice margin, such as Nordenskiöld Gletscher. Although given the synchronicity of outlet glacier response to changes in climate on millennial to centennial timescales, we infer that the lag in ice margin response of slow flowing, land-based, sectors of the ice margin is likely a decadal-scale phenomenon.

Conclusion

This study details the pattern and timing of middle- to late-Holocene ice margin fluctuations at Sermeq Kujatdleq and Nordenskiöld Gletscher in the Disko Bugt region. We add to a growing database that documents GrIS change during the Holocene. In both systems, the GrIS margin retreated to near its present ice margin configuration at ~7–8 ka. Both glaciers remained in a smaller-than-present extent until ~500 years ago, when they advanced into the catchment of currently proglacial lakes. Using geologic, historical, and remote-sensing records, we note the asynchronous behavior of the two outlet glaciers in the 20th century, with Sermeq Kujatdleq achieving a maximum late-Holocene extent between AD 1992 and 1994, and undergoing subsequent retreat. Nordenskiöld Gletscher has remained in the proglacial lake's catchment for the past 500 years, with the possible exception during the past 200 years. Historical records indicate that the Nordenskiöld Gletscher terminus has been advancing from the AD 1950s through the present.

These records, in addition to those from Sarqardlíp Sermia and Jakobshavn Isbræ, demonstrate relative synchronicity (within dating resolution) in retreat and advance of the GrIS margin on millennial and centennial timescales. Yet, the four glacier systems in the Disko Bugt region behave asynchronously on decadal timescales. We propose that this asynchronicity in decadal-scale ice margin fluctuations is because of variability in the response time of differing sectors of the GrIS driven by local velocity and internal ice dynamics. These findings demonstrate the need for additional high-resolution records of ice margin change that extend beyond the scope of the historical records to aid in better predictions of ice retreat in response to climate change and subsequent future sea-level rise.

Acknowledgements

We thank Mathew McClellan, Brayton West, and Sylvia Choi for invaluable assistance in the laboratory; O Bennike for assistance

in macrofossil identification; CH2M Hill Polar Field Services for help with field logistics; the 109th Air National Guard for transportation to and from Greenland; and Lena Håkansson for aerial photographs. We thank Meredith Kelly, Laura Levy, and three other anonymous reviewers for helpful comments that improved our manuscript.

Funding

This work was supported by NSF grant 1156361.

ORCID iD

Samuel E Kelley  <https://orcid.org/0000-0001-9214-0577>

References

- Bamber JL, Alley RB and Joughin I (2007) Rapid response of modern day ice sheets to external forcing. *Earth and Planetary Science Letters* 257: 1–13.
- Bennike O, Anderson NJ and McGowan S (2010) Holocene palaeoecology of southwest Greenland inferred from macrofossils in sediments of an oligosaline lake. *Journal of Paleolimnology* 43: 787–798.
- Briner JP, Kaufman DS, Bennike O et al. (2014) Amino acid ratios in reworked marine bivalve shells constrain Greenland Ice Sheet history during the Holocene. *Geology* 42: 75–78.
- Briner JP, Stewart H, Young N et al. (2010) Using proglacial-threshold lakes to constrain fluctuations of the Jakobshavn Isbræ ice margin, western Greenland, during the Holocene. *Quaternary Science Reviews* 29: 3861–3874.
- Briner JP, Young N, Thomas E et al. (2011) Varve and radiocarbon dating support the rapid advance of Jakobshavn Isbræ during the Little Ice Age. *Quaternary Science Reviews* 30: 2476–2486.
- Christoffersen M (1974) *Quaternary Map of Greenland: Sønder Strømfjord-Nûgssuaq Kvartærgeologisk; Sheet 3*. Copenhagen: Greenland Geologic Survey.
- Cronauer SL, Briner JP, Kelley SE et al. (2016) ¹⁰Be dating reveals early-middle Holocene age of the Drygalski Moraines in central West Greenland. *Quaternary Science Reviews* 147: 59–68.
- Csatho BM, Schenk AF, Van Der Veen CJ et al. (2014) Laser altimetry reveals complex pattern of Greenland Ice Sheet dynamics. *Proceedings of the National Academy of Sciences of the United States of America* 111: 18478–18483.
- Csatho BM, Schenk T, Van Der Veen CJ et al. (2008) Intermittent thinning of Jakobshavn Isbræ, West Greenland, since the Little Ice Age. *Journal of Glaciology* 54: 131–144.
- Daigle TA and Kaufman DS (2009) Holocene climate inferred from glacier extent, lake sediment and tree rings at Goat Lake, Kenai Mountains, Alaska, USA. *Journal of Quaternary Science* 24: 33–45.
- Hua Q (2009) Radiocarbon: a chronological tool for the recent past. *Quaternary Geochronology* 4: 378–390.
- Hua Q and Barbetti M (2004) Review of tropospheric bomb (super 14) C data for carbon cycle modeling and age calibration purposes. *Radiocarbon* 46: 1273–1298.
- Hua Q and Barbetti M (2007) Influence of atmospheric circulation on regional ¹⁴CO₂ differences. *Journal of Geophysical Research* 112: D19.
- Hua Q, Barbetti M and Rakowski AZ (2013) Atmospheric radiocarbon for the period 1950–2010. *Radiocarbon* 55: 2059–2072.
- Joughin I, Smith B, Shean D et al. (2014) Brief communication: Further summer speedup of Jakobshavn Isbræ. *The Cryosphere* 8: 209–214.
- Kaplan MR, Wolfe AP and Miller GH (2002) Holocene environmental variability in southern Greenland inferred from lake sediments. *Quaternary Research* 58: 149–159.

- Kaplan MR, Hein AS, Hubbard A et al. (2009) Can glacial erosion limit the extent of glaciation? *Geomorphology* 103: 172–179.
- Karlén W (1976) Lacustrine sediments and tree-limit variations as indicators of Holocene climatic fluctuations in Lappland, northern Sweden. *Geografiska Annaler: Series A, Physical Geography* 58: 1–34.
- Kaufman DS, Schneider DP, McKay NP et al. (2009) Recent warming reverses long-term Arctic cooling. *Science* 325: 1236–1239.
- Kelley SE, Briner JP and Young NE (2013) Rapid ice retreat in Disko Bugt supported by ^{10}Be dating of the last recession of the western Greenland Ice Sheet. *Quaternary Science Reviews* 82: 13–22.
- Kelley SE, Briner JP and Zimmerman SR (2015) The influence of ice marginal setting on early Holocene retreat rates in central West Greenland. *Journal of Quaternary Science* 30: 271–280.
- Kelley SE, Briner JP, Young NE et al. (2012) Maximum late Holocene extent of the western Greenland Ice Sheet during the late 20th century. *Quaternary Science Reviews* 56: 89–98.
- Kelly M (1980) *The Status of the Neoglacial in Western Greenland*. Copenhagen: Grønlands Geologiske Undersøgelse.
- Kjær KH, Khan SA, Korsgaard NJ et al. (2012) Aerial photographs reveal late-20th-century dynamic ice loss in north-western Greenland. *Science* 337: 569–573.
- Larsen NK, Funder S, Kjær KH et al. (2014) Rapid early Holocene ice retreat in West Greenland. *Quaternary Science Reviews* 92: 310–323.
- Lesnek AJ and Briner JP (2018) Response of a land-terminating sector of the western Greenland Ice Sheet to early Holocene climate change: Evidence from ^{10}Be dating in the Søndre Isortoq region. *Quaternary Science Reviews* 180: 145–156.
- Levy LB, Kelly MA, Howley JA et al. (2012) Age of the Ørkenalalen moraines, Kangerlussuaq, Greenland: Constraints on the extent of the southwestern margin of the Greenland Ice Sheet during the Holocene. *Quaternary Science Reviews* 52: 1–5.
- Levy LB, Larsen N, Davidson T et al. (2017) Contrasting evidence of Holocene ice margin retreat, south-western Greenland. *Journal of Quaternary Science* 32: 604–616.
- Lloyd J, Moros M, Perner K et al. (2011) A 100 yr record of ocean temperature control on the stability of Jakobshavn Isbræ, West Greenland. *Geology* 39: 867–870.
- Long AJ, Roberts DH and Wright MR (1999) Isolation basin stratigraphy and Holocene relative sea-level change on Arveprinsen Ejlund, Disko Bugt, West Greenland. *Journal of Quaternary Science* 14: 323–345.
- Long AJ, Woodroffe SA, Dawson S et al. (2009) Late Holocene relative sea level rise and the Neoglacial history of the Greenland ice sheet. *Journal of Quaternary Science* 24: 345–359.
- Long AJ, Woodroffe SA, Roberts DH et al. (2011) Isolation basins, sea-level changes and the Holocene history of the Greenland Ice Sheet. *Quaternary Science Reviews* 30: 3748–3768.
- Meier MF, Dyurgerov MB, Rick UK et al. (2007) Glaciers dominate eustatic sea-level rise in the 21st century. *Science* 317: 1064–1067.
- Nesje A (1992) A piston corer for lacustrine and marine sediments. *Arctic and Alpine Research* 24: 257–259.
- Nye J (1960) The response of glaciers and ice-sheets to seasonal and climatic changes. *Proceedings of the Royal Society of London: Series A, Mathematical and Physical Sciences* 256: 559–584.
- Pfeffer WT, Harper JT and O’Neel S (2008) Kinematic constraints on glacier contributions to 21st-century sea-level rise. *Science* 321: 1340–1343.
- Price SF, Payne AJ, Howat IM et al. (2011) Committed sea-level rise for the next century from Greenland ice sheet dynamics during the past decade. *Proceedings of the National Academy of Sciences of the United States of America* 108: 8978–8983.
- Rasch M (2000) Holocene relative sea level changes in Disko Bugt, West Greenland. *Journal of Coastal Research* 16: 306–315.
- Rasch M and Jensen JF (1997) Ancient Eskimo dwelling sites and Holocene relative sea-level changes in southern Disko Bugt, central West Greenland. *Polar Research* 16: 101–115.
- Reimer PJ, Brown TA and Reimer RW (2004) Discussion: reporting and calibration of post-bomb ^{14}C data. *Radiocarbon* 46: 1299–1304.
- Reimer PJ and Reimer RW (2011) CALIBomb radiocarbon calibration program.
- Rignot E and Kanagaratnam P (2006) Changes in the velocity structure of the Greenland ice sheet. *Science* 311: 986–990.
- Rignot E and Mouginot J (2012) Ice flow in Greenland for the international polar year 2008–2009. *Geophysical Research Letters* 39: L11501. DOI: 10.1029/2012GL051634.
- Rignot E, Koppes M and Velicogna I (2010) Rapid submarine melting of the calving faces of West Greenland glaciers. *Nature Geoscience* 3: 187–191.
- Stocker TF, Dahe Q and Plattner G-K (2013) Summary for policymakers. Climate change 2013: The physical science basis. Working Group I, Contribution to the Fifth Assessment Report, Intergovernmental Panel on Climate Change (IPCC), Geneva.
- Stuiver M, Reimer P and Reimer R (2010) CALIB 7.1 program. Available at: <http://calib.org> (accessed 1 June 2017).
- Weidick A (1968) Observations on some Holocene glacier fluctuations in west Greenland. *Meddeleser Om Grønland* 165: 1–202.
- Weidick A (1993) Neoglacial change of ice cover and the related response of the Earth’s crust in West Greenland. *Rapport Grønlands Geologiske Undersøgelse* 159: 121–126.
- Weidick A (1994) Historical fluctuations of calving glaciers in south and West Greenland. *Rapport Grønlands Geologiske Undersøgelse* 161: 73–79.
- Weidick A (1996) Neoglacial changes of ice cover and sea level in Greenland—a classical enigma. In: Grønnow B (ed.) *The Paleo-Eskimo Cultures of Greenland* Copenhagen: Danish Polar Center University of Copenhagen, pp. 257–270.
- Weidick A and Bennike O (2007) *Quaternary Glaciation History and Glaciology of Jakobshavn Isbræ and the Disko Bugt Region, West Greenland: A Review*. Copenhagen: Geological Survey of Denmark and Greenland.
- Yoshimori M and Abe-Ouchi A (2012) Sources of spread in multimodel projections of the Greenland Ice Sheet surface mass balance. *Journal of Climate* 25: 1157–1175.
- Young NE and Briner JP (2015) Holocene evolution of the western Greenland Ice Sheet: Assessing geophysical ice-sheet models with geological reconstructions of ice-margin change. *Quaternary Science Reviews* 114: 1–17.
- Young NE, Briner JP, Rood DH et al. (2013) Age of the Fjord Stade moraines in the Disko Bugt region, western Greenland, and the 9.3 and 8.2 ka cooling events. *Quaternary Science Reviews* 60: 76–90.